Langmuir

Article

pubs.acs.org/Langmuir

Variable Range Hopping in Single-Wall Carbon Nanotube Thin Films: A Processing−Structure−Property Relationship Study

Sida Luo,[†] Tao Liu,*[,†] Shermane M. Benjamin,[‡] and James S. Brooks[‡]

[†]High-Performance Materials Institute, FAMU-FSU College of Engineering, Florida State University, 2525 Pottsdamer Street, Tallahassee, Florida 32310, United States

[‡]National High Magnetic Field Laboratory, Florida State University, Tallahassee, Florida 32310, United States

Supporting Information

ABSTRACT: By varying the ultrasonication and ultracentrifugation conditions, single-walled carbon nanotube (SWCNT) dispersions with a broad range of SWCNT length and diameter (L = 342−3330 nm; d = 0.5−12 nm) were prepared and characterized by a preparative ultracentrifuge method (PUM) and dynamic light scattering (DLS) technique. The well-characterized dispersions were then fabricated into SWCNT thin films by spray coating. Combined optical, spectroscopic, and temperature-dependent electrical measurements were performed to study the effect of SWCNT structures on the charge transport behavior of SWCNT thin films. Regardless of SWCNT size in the dispersion and the thin film thickness, the three-dimensional variable range hopping (3D VRH) conduction model was found to be appropriate in explaining the temperature-dependent sheet resistance results for all SWCNT thin films prepared in this study. More importantly, with the SWCNT structural information determined by the PUM method, we were able to identify a strong correlation between the length of SWCNTs and the 3D VRH parameter T_0, the Mott characteristic temperature. When the SWCNT length is less than ∼700 nm, the T_0 of SWCNT thin films shows a drastic increase, but when the length is greater than ∼700 nm, T_0 is only weakly dependent on the SWCNT length. Under the framework of traditional VRH, we further conclude that the electron localization length of SWCNT thin films shows a similar dependence on the SWCNT length.

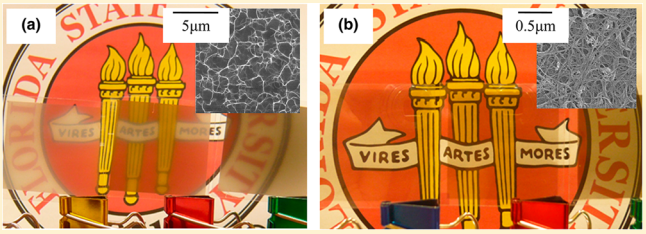

INTRODUCTION

As a cost-effective and mass-producible platform, single-wall carbon nanotube (SWCNT) thin films—quasi-two-dimensional (quasi-2D) networks formed by random entanglement of individual tubes and/or SWCNT bundles[1]—have been found valuable for developing a variety of different applications, such as thin film transistors,[2] transparent conductive electronics,[3] field emission devices,[4] electrochemical energy conversion and storage devices,[5] strain,[6] and gas sensors.[7] In all these SWCNT thin film-based devices, the behavior of charge carrier transport across the SWCNT network plays a critical role in determining the device performance. Studies on the temperature, electric field and magnetic field dependent electrical conductivity of SWCNT networks[8,13] provide strong evidence that variable range hopping (VRH) is responsible for the electrical charge transport in thin SWCNT networks. Different types of disorder existing in the SWCNT network, such as vacancies and structural defects of individual tubes and tube/tube contacts, presumably play critical roles for the localization of electronic states that result in the hopping transport of charge carriers.[14,15] The charge transport behavior of a SWCNT thin film is closely related to its detailed chemical/physical structure, which can be modified and even tailored through varying the film preparation/processing/post-treatment conditions. In this regard, Kaiser et al.[16−18] performed a series of systematic studies to clarify the role of film thickness, chemical doping and ion irradiation on the charge transport mechanism(s) in SWCNT network. Recently, Yanagi et al.[19] utilized metallic (M-SWCNT) and semiconducting (S-SWCNT) enriched SWCNTs to prepare SWCNT thin films with controlled composition of the ratio of M-SWCNTs to S-SWCNTs (MS ratio). It was found that, with increasing the MS ratio, the transport of charge carriers in SWCNT thin film can change from quantum transport, VRH, to Efros-Shklovskii VRH (ES-VRH). The ES-VRH model[20] is different from the traditional Mott VRH[21] in that the Coulomb interactions between localized electrons are considered. The work of Yanagi et al. suggested that the Schottky barriers formed between metallic and semiconducting SWCNTs are the possible origins for strong disorder existing in SWCNT thin films. Additionally, another source of disorder might be due to the random distribution of nanotube diameters and the resulted inconsistent band gap energies.

Among the different methods for fabricating SWCNT thin films, such as vacuum filtration,[22] spin coating,[23] and dip-coating,[24] SWCNT dispersion is typically required. In the

Received: April 3, 2013
Revised: May 31, 2013
Published: June 10, 2013

dx.doi.org/10.1021/la401264r | Langmuir 2013, 29, 8694−8702

Table 1. Important Processing and Structural Information of SWCNT Dispersions and SWCNT Thin Films

sample name	sonication duration (hrs)	centrifuge force ($\times 10^3$ g-force)	sedimentation coefficient ($\times 10^{-13}$ s)	diffusion coefficient ($\times 10^{-8}$ cm^2/sec)	average length (nm)	average diameter (nm)	3D VRH T_0 (K)	
							T_0^{min}[a]	$\langle T_0 \rangle$[b]
S-0.5hr	0.5	0	403.1	0.89	3330.3	12.0	46204	49037 ± 4006
S-1hr	1	0	382.6	1.11	2570.8	11.9	45309	52293 ± 9876
S-2hr	2	0	112.1	1.50	2030.1	6.2	57850	65054 ± 10188
S-4hr	4	0	37.5	2.79	1074.1	3.6	65470	60923 ± 6431
S-10hr	10	0	34.1	4.79	557.0	3.7	95063	97672 ± 3689
S-30hr	30	0	14.9	6.20	447.2	2.4	152380	156655 ± 6046
SC-0.5hr-30kg	0.5	30	10.9	3.80	842.2	1.9	50386	58536 ± 11525
SC-1hr-40kg	1	40	15.5	4.67	632.0	2.4	45008	47572 ± 3625
SC-2hr-50kg	2	50	7.0	5.39	578.5	1.5	57459	54757 ± 3822
SC-4hr-70kg	4	70	3.0	6.94	464.9	1.0	83571	81846 ± 2440
SC-10hr-100kg	10	100	7.1	8.19	346.1	1.6	89822	95326 ± 7784
SC-30hr-200kg	30	200	0.9	9.91	341.5	0.5	183240	201565 ± 25915

[a] T_0^{min} - Mott's characteristic temperature for the thin film with highest optical absorbance/thickness that is processed from a given dispersion. [b] $\langle T_0 \rangle$ - averaged T_0 calculated with the two samples that have the highest optical absorbance/thickness, which is an approximate measure of the thickness-independent T_0.

dispersion preparation, the size of SWCNTs is subject to the processing conditions. Then, an interesting question is raised: How is the SWCNT size in the dispersion related to the electrical properties and the charge transport behavior of SWCNT thin films? A few recent studies have attempted to answer the first part of this question.[25−28] Dispersions with different SWCNT bundle lengths L_{av}, can be prepared by varying the sonication conditions. Hecht et al.[25] found a power-law dependence of the electrical conductivity of SWCNT thin films on $L_{av} - \sigma_{dc} \sim L_{av}^{1.46}$. Shin et al.[27] applied the ultracentrifugation process to tailor the SWCNT bundle diameter D_{av} in the dispersion and established a similar power-law dependence of the electrical conductivity of SWCNT thin film on $D_{av} - \sigma_{dc} \sim D_{av}^{-1.613}$. Given the progress made in understanding the processing-structure-electrical property relationships of SWCNTs, however, the effect of SWCNT size in the dispersion on the charge transport behavior of SWCNT thin films is lacking, and this is the subject of the present paper. Specifically, with varied ultrasonication and ultracentrifugation conditions, a broad range of SWCNT length and diameter (L = 342 − 3330 nm; d = 0.5 − 12 nm) in SWCNT dispersions were achieved and then characterized by a preparative ultracentrifuge method (PUM) and dynamic light scattering (DLS).[29] The well-characterized dispersions were then fabricated into SWCNT thin films by spray coating. Regardless of SWCNT size in the dispersion and the thin film thickness, the three-dimensional (3D) VRH conduction model was found to be appropriate in explaining the temperature-dependent sheet resistance for all the SWCNT thin films prepared in this study. More importantly, with the SWCNT structural information determined by the PUM method, we were able to identify a strong correlation between the length of SWCNTs and the 3D VRH parameter T_0, the Mott characteristic temperature. When the SWCNT length is less than ∼700 nm, the T_0 of SWCNT thin films shows a drastic increase, but when the length is greater than ∼700 nm, the T_0 is only weakly dependent on the SWCNT length. Under the framework of traditional VRH, we also find that the electron localization length of SWCNT thin film has a similar dependence on the SWCNT length.

EXPERIMENTAL SECTION

Preparation and Characterization of SWCNT Dispersions. Purified SWCNTs (HiPco SWCNTs, PO# 355) were purchased from Carbon Nanotechnologies, Inc. Sodium dodecylbenzensulfonate (SDBS, CAS # 25155-30-10) was supplied by Sigma-Aldrich. With these as-received chemicals and by following the procedures described previously,[29] a series of SWCNT aqueous dispersions with varied SWCNT bundle length and diameter were prepared. In brief, a mixture of 16 mg SWCNTs and 100 mL H_2O/SDBS solution (0.7 wt % SDBS in concentration) was sonicated in an ice bath by using a Misonix 3000 horn sonicator. The sonicator was operated at 20 kHz in a pulse operation mode (on 10 s, off 30 s) with the power level set at 45 W. By varying the effective sonication time (0.5, 1, 2, 4, 10, and 30 h), a total of six as-sonicated SWCNT dispersions were obtained. They were respectively denoted as S-0.5hr, S-1hr, S-2hr, S-4hr, S-10hr, and S-30hr. Each of the as-sonicated SWCNT dispersions was further subjected to an ultracentrifugation process for 2 h using an Optima MAX-XP benchtop ultracentrifuge (Beckman Coulter, MLS-50 swinging bucket rotor) at a constant g-force acceleration. At the end of centrifugation process, the supernatant was carefully decanted and collected. The dispersions obtained were denoted respectively by SC-0.5hr-30 kg, SC-1hr-40 kg, SC-2hr-50 kg, SC-4hr-70 kg, SC-10hr-100 kg, and SC-30hr-200 kg. In the nomenclature, the first and second number respectively indicates the effective sonication duration and the centrifugation g-force used for dispersion preparation.

We have recently developed a PUM[29,30] for quantitative determination of the sedimentation behavior of SWCNT dispersions. With the Optima MAX-XP ultracentrifuge and a fixed angle rotor (30°, TLA-100.3), the PUM was performed to all the dispersions prepared in this study. The resulting sedimentation coefficients, s, which characterizes the sedimentation velocity of SWCNTs under a unit centrifugal field, are given in Table 1.

A Delsa Nano C (Beckman Coulter, Inc., scattering angle of 165°, excitation laser wavelength of 658 nm) was used to perform DLS measurements for all the SWCNT dispersions. The recorded time correlation function of the scattered light intensity was analyzed by the

dx.doi.org/10.1021/la401264r | Langmuir 2013, 29, 8694−8702

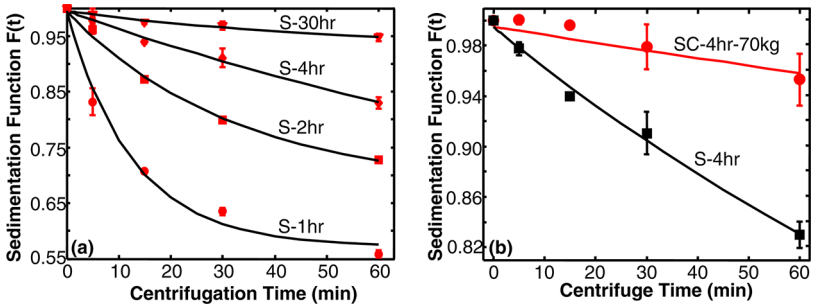

Figure 1. Representative sedimentation functions of SWCNT dispersions. (a) Effect of sonication duration. (b) Effect of centrifugation process on the as-sonicated dispersion. S for as-sonicated dispersion; SC for sonication and centrifugation processed dispersion. Scattered data points are the experimental results; the smooth lines are the corresponding theoretical fits.

CONTIN method[31,32] to determine the diffusion coefficient D of SWCNTs in the dispersion.

With the sedimentation coefficient s determined by PUM and the diffusion coefficient D measured by DLS, the bulk averaged length L and diameter d of SWCNTs in a given dispersion can be calculated according to the hydrodynamic model of rigid rods given by Yamakawa:[29,33]

$$s = \frac{(\upsilon^{-1} - \rho)d^2}{12\eta}\left(\ln\frac{L}{d} + 2\ln 2 - 1\right) \quad (1)$$

$$D = \frac{kT}{3\pi\eta L}\left(\ln\frac{L}{d} + 2\ln 2 - 1\right) \quad (2)$$

where υ is the partial specific volume of the dispersed particle, ρ is the density of the solvent, η is the viscosity of the liquid medium, k is the Boltzmann constant, and T is the temperature.

Fabrication and Characterization of SWCNT Thin Films. A spray coating technique was carried out to fabricate the SWCNT thin films. In brief, an Iwata Eclipse HP-BS airbrush with a jet compressor operated at 200 kPa was used to deposit an appropriate amount of SWCNT dispersion onto a biaxially oriented polyethylene terephthalate (PET) substrate (ES301450, 0.25 mm in thickness, Goodfellow Corp.). To accelerate water evaporation and facilitate thin film formation, the PET substrate was heated by a hot plate (1000-1 Precision Hot Plate, Electronic Micro Systems Ltd.) at 85 °C. In the spray process, the spray gun was manually controlled such that the deposition of SWCNT dispersion was confined in a 4 cm × 4 cm area on the PET substrate, resulting in a SWCNT thin film with a similar shape. In addition, the thickness of SWCNT thin film was tailored by varying the amount of SWCNT dispersion being sprayed, which was respectively selected at 5 mL, 10 mL, 20 and 40 mL. The as-deposited SWCNT thin film obtained from the spray coating process was further subjected to an immersion treatment in deionized H_2O overnight to remove the residual SDBS molecules. With energy dispersive X-ray spectroscopy (EDX) as an examination tool, in our recently published work, this protocol has been proved sufficient to remove SDBS molecules.[34] The immersion-treated SWCNT thin film was then subsequently dried in air at ambient temperature prior to electrical and structural characterization.

In the spray coating process, only part of the SWCNT dispersion is deposited onto the PET substrate, resulting in a low SWCNT yield. In order to estimate the SWCNT loss during the spray coating process, a solution-cast method that allows 100% utilization of SWCNTs was selected as a control to prepare SWCNT thin films. In brief, an appropriate amount (1, 3, 5, 7.5, and 10 mL) of a selected SWCNT dispersion (S-0.5hr) was mixed with 3 mL of a polyvinylpyrrolidone (PVP)/H_2O solution (M_w of PVP = 1300K, Aldrich, 1 wt % in concentration) to form a homogeneous SWCNT/PVP/H_2O ternary solution. The mixture was then cast into a glass mold (W x L x H = 5 cm ×5 cm ×1 cm) at ambient temperature. After water evaporation and drying, the homogeneous SWCNT/PVP films were used as the control/standard for estimating the SWCNT loss involved in spray coating process. The results on the estimation of spray coating efficiency are given in the Supporting Information.

Scanning electron microscopy (SEM) was performed with JEOL 7400 at 10 kV to examine the microstructures/morphologies of SWCNT thin films. The thin film sample was sputter coated with gold prior to SEM imaging.

A Varian Cary 5000 UV−vis−NIR spectrometer was used to record the optical absorption spectra of SWCNT thin films in the range of 300 to 1300 nm. For each thin film sample, a total of five locations were randomly selected for the optical absorption measurement. To eliminate the substrate contribution to the optical absorption of SWCNT thin film, blank PET was used as the reference in the measurement. In addition, the measurement was also performed with air as the reference for comparison. The optical absorbance of SWCNT thin films measured with the PET film and air as the respective reference shows an excellent linear correlation, which is given by Abs(PET BG at 550 nm) = 0.998 × Abs(Air BG at 550 nm) − 0.153.

A Renishaw inVia Raman microscope was used for collecting the Raman spectra of SWCNT thin films with a 785 nm excitation laser in backscattering geometry. According to the previous studies,[35,36] the integrated intensity of the radial-breathing mode (RBM) at 267 cm^{-1} normalized by the G-band at 1593 cm^{-1} ($I_{RBM\text{-}267}/I_G$) provides valuable information regarding he bundling states of SWCNTs in the thin film.

An LC-1 Liquid Nitrogen Cryostat System (Advanced Research Systems Inc.) equipped with a Lakeshore 325 temperature controller, Keithley 6221 current source, Keithley 2182A nanovoltmeter and Agilent 3499B switch/control system was used to examine the temperature-dependent electrical resistance of SWCNT thin films (100−300 K). The sample to be tested was cut into a square shape of 1 cm × 1 cm and then fixed onto a LakeShore 700RSH 4-lead resistance sample holder. Four copper wire electrodes were respectively connected to the four corners of the sample with silver paste. This configuration allows an implementation of the standard van der Pauw method for electrical resistance measurements. For a few selected SWCNT thin film samples, the electrical resistance in a much broader temperature range (12−300 K) was also measured with a conventional vacuum jacketed liquid helium cryostat and probe. In these measurements, a traditional 4-terminal in-line electrode configuration was prepared by painting four parallel silver paste lines on the sample surface. Gold wires of 0.025 mm in diameter were used for connecting the silver electrodes to the probe, which was connected to a with Keithley 6517a electrometer and Keithley Model 220 DC current source. The sample temperature was controlled by helium exchange gas between the cryostat sample chamber and the 4.2 K liquid helium bath level, and measured with a Cernox calibrated resistive thermometer using a Lakeshore Temperature Controller.

RESULTS AND DISCUSSION

Structure Characterization of SWCNT Dispersion. The PUM[29] allows the experimental determination of the sedimentation function of a given SWCNT dispersion. The

dx.doi.org/10.1021/la401264r | Langmuir 2013, 29, 8694−8702

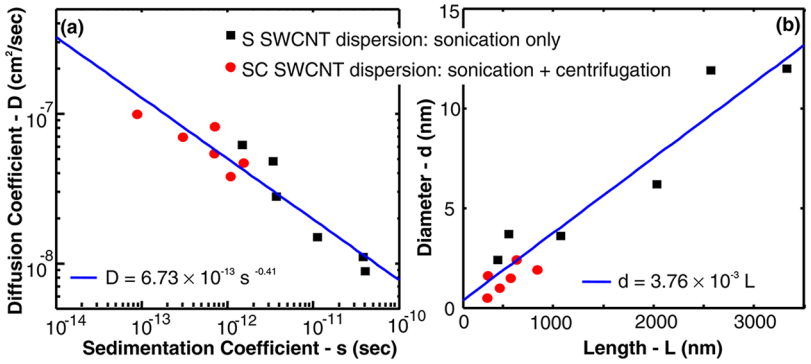

Figure 2. The relationship between (a) diffusion (D) and sedimentation (s) coefficients and (b) diameter (d) and length (L) of the SWCNT bundles in the dispersion processed by sonication and centrifugation process.

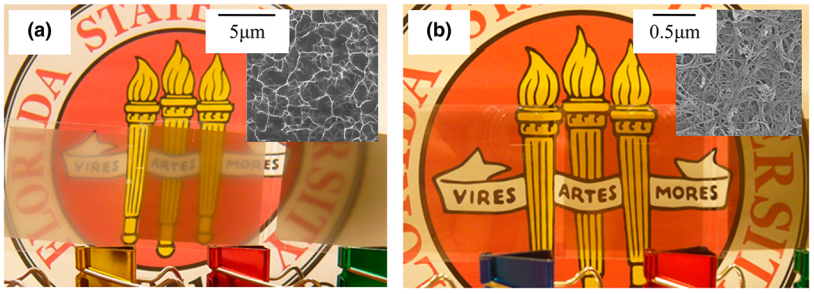

Figure 3. Photo and SEM images (inset) of representative SWCNT thin films using 2 h of sonicated dispersion (S-2hr) before (a) and after (b) immersion treatment.

sedimentation function is a measure of the SWCNT concentration reduction in a control volume when the dispersion is under the action of a centrifugal field for a certain period of time duration. As an example, Figure 1a compares the sedimentation functions of S-1hr, S-2hr, S-4hr, and S-30hr. It clearly shows that with increasing sonication time, the decay of the sedimentation function with respect to the centrifugation time slows down. This indicates the gradual size reduction of SWCNT particles with increasing the sonication duration. When the as-sonicated SWCNT dispersion is subjected to the ultracentrifugation process, a further reduction in size of the SWCNT particles left in the supernatant is expected due to the precipitation of large-sized SWCNT particles. With S-4hr and SC-4hr-70 kg as representative examples, this fact is clearly reflected through the sedimentation function measurements as shown in Figure 1b.

On the basis of the sedimentation model established by Mason and Shiragami,[37,38] the sedimentation function can be theoretically fit to obtain the bulk averaged sedimentation coefficient s of SWCNT particles, and s values obtained in this way for all the dispersions are listed in Table 1 for comparison. In the same Table, the diffusion coefficients of SWCNT particles D measured by DLS were also given. With the PUM determined sedimentation coefficient s and the DLS measured diffusion coefficient D, the bulk averaged length- L and diameter d of SWCNTs bundles for each dispersion were calculated according to eqs 1 and 2. The results are also given in Table 1.

From the results listed in Table 1, we plotted D against s in Figure 2a for the as-sonicated and the centrifugation-separated SWCNT dispersions. The size reduction of SWCNT particles with increasing sonication duration or centrifugation g-force is evidenced by the corresponding decreased (increased) sedimentation (diffusion) coefficient. Additionally, an approximate power-law relationship between D and s for both processes can be identified: $D \propto s^{-\beta}$ with the numerical value of $\beta = 0.41$. When inspecting eq 1 and 2, the power-law relationship between D and s is not immediately apparent. Nevertheless, with the relations $s \propto d^2$ and $D \propto L^{-1}$ as suggested by eqs 1 and 2, one can conclude that the experimentally observed relationship $D \propto s^{-0.41}$ is due to a strong correlation existing between the length L and diameter-d of SWCNTs bundles. Specifically, we have $L \propto d^{0.82}$. This strong correlation between L and d was born out as shown in Figure 2b, where we plotted d against L by using the results listed in Table 1. The strong correlation between d and L confirms that the SWCNT size reduction is a convoluted result of decrease in both length and diameter of SWCNT particles. For the sonication process, the strong correlation between d and L is due to the simultaneously occurred length shortening and bundle exfoliation effects. In the centrifugation process, the precipitation of long and large diameter SWCNTs results in short and thin SWCNTs in the supernatant, which have a strong correlation between their length and diameter. This suggests that the centrifugation process is not able to separate the SWCNTs by length and diameter independently. The experimental evidence provided here is in conflict with the key assumption made in Shin's work,[27] in which they report that a constant bundle length can be obtained with centrifugation.

Effect of Immersion-Drying on the SWCNT Thin Film Morphologies. As described in the Experimental Section, an immersion-drying process is normally applied to the as-sprayed SWCNT thin films. This step is necessary for the final formation of high-quality, uniform, and transparent SWCNT thin films. Figure 3a,b respectively show pictures of the as-sprayed and the immersion-drying-treated SWCNT thin films. Apparently, the as-sprayed thin films appear hazy and translucent. However, after immersion-drying treatment, the

dx.doi.org/10.1021/la401264r | Langmuir 2013, 29, 8694−8702

thin films become more transparent. In addition to the visual appearance, the microscopic packing structures of SWCNTs in the as-sprayed and immersion-drying treated films also show significant difference. The SEM micrographs shown in the insets of Figure 3a,b clearly indicate the transformation of the loosely packed 3D SWCNT networks in the as-sprayed film into a densely packed quasi-2D SWCNT network after immersion-drying treatment. Due to the lossely packed SWCNT network structures and the presence of insulating SDBS molecules, the as-spray thin films was barely conductive. The hazy appearance of the as-sprayed thin films is related to their loosely packed 3D SWCNT network structures, which induce the refractive index inhomogeneity and lead to excess light scattering. Such inhomogeneity is greatly suppressed in the immersion-drying treated thin films to impart their high transparancy.

SWCNT bundles, in which the individual tubes are organized in a quasi-2D hexagonal lattice, naturally form in the carbon nanotube growth processes due to the strong intertube van der Waals interactions.[39] Heller et al.[36] first established using the G-band normalized 267 cm^{-1} RBM band intensity (I_{267}/I_G) as an indicator for characterizing the bundling states of SWCNTs when the sample is excited by 785 nm laser. This result was corroborated by us with the simultaneous Raman scattering and photoluminescence spectroscopy method.[35] With I_{267}/I_G as an indicator, we examined the bundling states of SWCNTs for all the thin film samples and found an important and universal dependence of I_{267}/I_G on the quantity $1/dL^2$ as shown in Figure 4. It is noted that d and L are respectively the diameter and

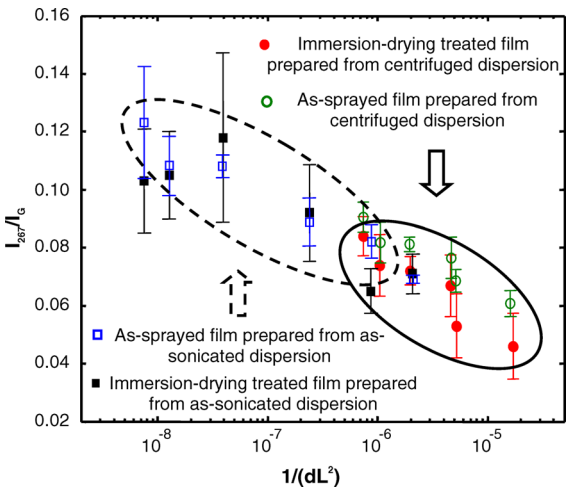

Figure 4. Relationship between the bundling state indicator I_{267}/I_G and the SWCNT packing parameter $1/dL^2$ for SWCNT thin films prepared under different conditions.

length of SWCNTs in the dispersion that was used for fabricating the thin film;, and dL^2 is the orientationally averaged excluded volume of SWCNTs. According to Philipse's thin rod packing theory,[40,41] $1/dL^2$ is proportional to the SWCNT packing density in the thin film.

The results shown in Figure 4 reveal a strong correlation between I_{267}/I_G and the size of SWCNT bundles in the dispersion that is used for fabricating the thin films. The I_{267}/I_G values of the thin films fabricated from the centrifuged dispersions (SC-series, smaller d and shorter L) are consistently less than those (S-series, larger d and longer L) prepared from the as-sonicated dispersions. In addition, for both SC- and S-series thin film samples, the immersion-drying treatment has a negligible influence on the value of I_{267}/I_G. The results shown in Figure 4 imply that the bundling states of SWCNTs in the thin film are mainly determined by the size of SWCNTs in the dispersion. The post-treatment process, e.g., immersion-drying, is able to modify the packing density and packing structures of SWCNTs (Figure 4) but not their bundling states.

Structure-Electrical Property Relationships of SWCNT Thin Films. The mechanism(s) of electronic transport in SWCNT network (films or fibers) have been intensively studied.[8,12,14,16,17,41−47] Among different models, the VRH was identified to be suitable for describing the electrical conduction of thin transparent SWCNT networks.[8−13] In agreement with these previous studies, we also found that the 3D VRH model is applicable in explaining the temperature-dependent electrical resistance for all the SWCNT thin films being investigated in this work. Moreover, the hopping parameters were found to be dependent upon the structures of SWCNT dispersion that was used in fabricating SWCNT thin films. More details are discussed below.

The VRH model was first developed by Mott[21] in considering the phonon-assisted tunneling transition of charge carriers between the localized states in the band gap of an amorphous semiconductor. The Mott's VRH model in 3D space suggests the temperature (T)-dependent conductivity σ as[48,49]

$$\sigma\sqrt{T} = \sigma_0 \exp\left[-\left(\frac{T_0}{T}\right)^{1/4}\right] \tag{3a}$$

$$\sigma_0 = \frac{e^2\nu_{ph}}{6}\sqrt{\frac{9N(E_F)\xi}{8\pi k_B}} \tag{3b}$$

$$T_0 = \frac{18.1}{\xi^3 N(E_F)k_B} \tag{3c}$$

where T_0 is the Mott characteristic temperature. As indicated by eqs 3b and 3c, the pre-exponential factor σ_0 and the characteristic temperature T_0 are related through $N(E_F)$, the electronic density of (localized) states at the Fermi level, and ξ, the localization length of the electronic wave functions. The parameters k_B, e, and ν_{ph} are respectively the Boltzmann constant, elementary electron charge and frequency of the phonons associated with the hopping process.

To apply eq 3 for studying the temperature-dependent sheet-resistance R and link the results to the optical absorbance A of the SWCNT thin films, we modified eq 3 with the relationship of $R = 1/\sigma t$ and $A = \varepsilon c t$ (t − thickness of the thin film; ε − the optical absorption cross-section of SWCNTs (cm^2/C-atom); c − the SWCNT packing density in the thin film in terms of the C-atom number density (C-atom/cm^3)). The modified result is given by

$$\frac{R}{\sqrt{T}} = R_0 \exp\left[\left(\frac{T_0}{T}\right)^{1/4}\right] \tag{4a}$$

$$R_0 = \frac{\varepsilon c}{A\sigma_0} \tag{4b}$$

For all the SWCNT thin film samples being studied here, eq 4a provides an excellent fit to the experimentally measured temperature-dependent resistance in the range of 100−300 K. Figure 5a presents the representative results of a linear plot of

dx.doi.org/10.1021/la401264r | Langmuir 2013, 29, 8694−8702

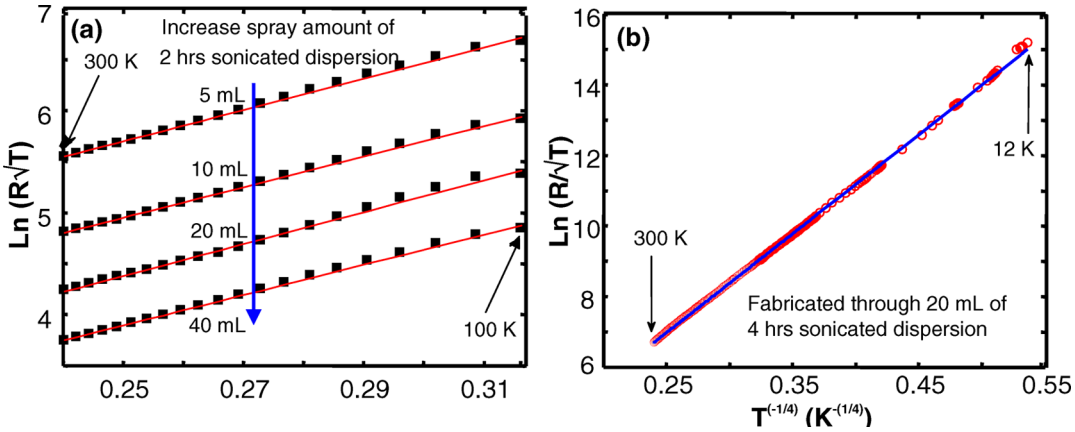

Figure 5. Temperature-dependent sheet resistance of representative SWCNT thin films evaluated by the standard van der Pauw method. (a) Thin films sprayed from varied amounts of 2 h as-sonicated dispersion (S-2hr) and measured in the range of 100−300K. (b) Thin films sprayed from 20 mL 4hr as-sonicated dispersion (S-4hr) and measured in the range of 12−300K. Scattered points are experimentally measured data, and the solid lines stand for the 3D VRH model fitting results according to eq 4a.

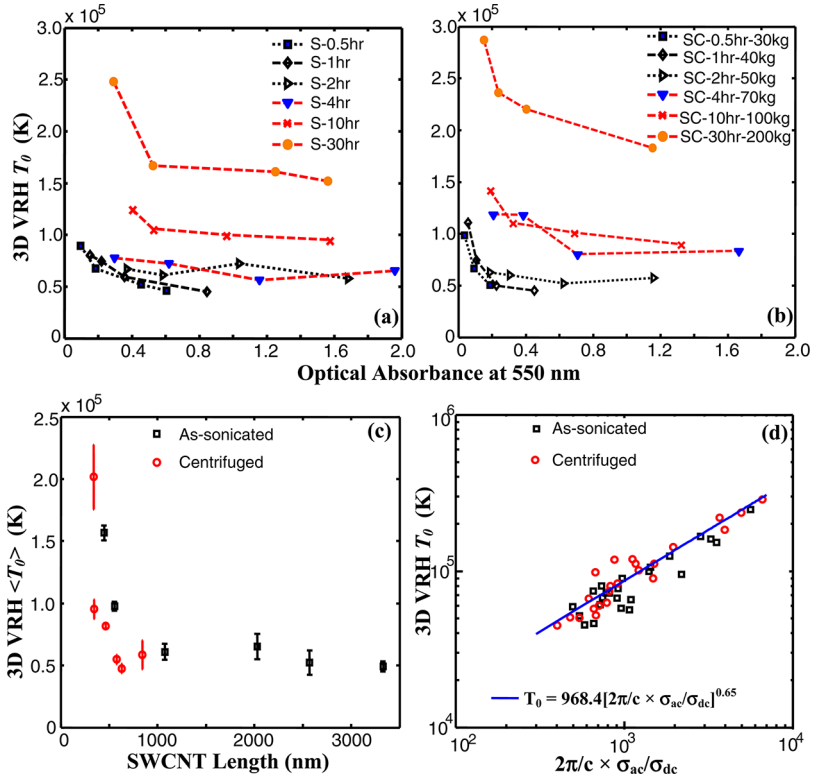

Figure 6. Thickness/optical absorbance dependent 3D VRH parameter T_0 of SWCNT thin films fabricated from (a) as-sonicated dispersion and (b) sonication + centrifugation processed dispersion. (c) Effect of SWCNT length on the thickness-independent 3D VRH parameter $\langle T_0 \rangle$. $\langle T_0 \rangle$ is listed in Table 1. (d) Comparison of Gruner's quality indicator σ_{ac}/σ_{dc} with the 3D VRH parameter T_0.

$\ln(R/\sqrt{T})$ vs $T^{-(1/4)}$ for the thin film samples sprayed with 2 h as-sonicated dispersion (S-2hr) at various amounts. The validity of 3D VRH for SWCNT thin films in a much broader temperature was further confirmed by fitting the electrical resistance measured in the range of 12−300 K for a few selected samples. Figure 5b provides the representative result. Again, the linear relationship between $\ln(R/\sqrt{T})$ and $T^{-(1/4)}$ as predicted by the 3D VRH model is clearly born out.

After establishing the 3D VRH as the mechanism for the charge carrier transport in SWCNT thin films, we are now in a position to investigate the effect of SWCNT structures in the dispersion as well as the film thickness on the hopping parameter, T_0. Using the optical absorbance at 550 nm as a measure of the thin film thickness, Figure 6a,b shows the thickness-dependent behavior of T_0 for the SWCNT thin films respectively processed from the as-sonicated and centrifuged dispersions. Clearly, regardless of the dispersion processing conditions, the T_0 of SWCNT thin film fabricated from the same dispersion shows a weak dependence on film thickness. Within the experimental errors, one can tell that, the thicker the thin film being fabricated, the smaller the T_0. Moreover, with increasing the film thickness, the T_0 of SWCNT thin film gradually decreases and eventually approaches a constant value. The observed thickness-dependent behavior of T_0 is a reflection

dx.doi.org/10.1021/la401264r | Langmuir 2013, 29, 8694−8702

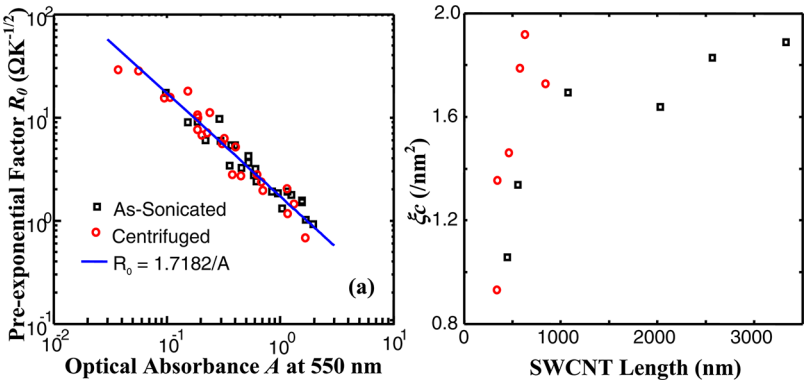

Figure 7. (a) Relationship between the optical absorption and the related 3D VRH pre-exponential factor R_0 for SWCNT thin films. (b) Effect of SWCNT length on the electron localization length of SWCNT thin films.

of the dependence of SWCNT packing density (number of tubes/bundles per unit volume) on the film thickness. At small thickness, the SWCNT packing density is low, which results in smaller electronic density $N(E_F)$ and thus higher T_0. With further increasing the film thickness, the SWCNT packing reaches a metastable randomly packed structure with a constant SWCNT packing density,[40,41] which then gives a constant or thickness-independent T_0. For each series of SWCNT thin films fabricated from a given dispersion, we used the two samples that have the highest optical absorbance/thickness to calculate the averaged T_0, which is designated by $\langle T_0 \rangle$, as an approximate measure of the thickness-independent T_0. The results are listed in Table 1. In the same table, the T_0 value for the sample with the highest optical absorbance/thickness was also listed and designated as T_0^{min}.

In addition to film thickness, the results shown in Figure 6a,b also clearly indicate that the sonication duration used for processing SWCNT dispersion has a strong effect on the T_0 of the correspondingly fabricated SWCNT thin film. At the same film thickness/optical absorbance, the longer the sonication duration, the higher the value of T_0. This observation suggests the critical role of SWCNT structures in the dispersion in dictating the VRH behavior of SWCNT thin films. With the SWCNT structural information determined by the PUM method (Table 1), we were able to identify a strong correlation between the length of SWCNTs and the thickness-independent 3D VRH parameter $\langle T_0 \rangle$. The results are shown in Figure 6c. Evidently, when the SWCNT length is less than ~700 nm, the $\langle T_0 \rangle$ of SWCNT thin films shows a drastic increase, but when the length is greater than ~700 nm, the $\langle T_0 \rangle$ is hardly dependent upon the SWCNT length. A plausible explanation for the observed SWCNT length-dependent $\langle T_0 \rangle$ is attributed to the coexisting and competitive inter- and intra- tube/bundle charge carrier transport in SWCNT thin films. The thin film composed of shorter (longer) tubes/bundles has higher (lower) number density of inter-tube/bundle contact. As a result, when SWCNTs are shorter, the inter-tube/bundle transport/tunneling events increase as compared to the transport along the tube/bundle. This has an effect raising the Mott's characteristic temperature T_0. The existence of a critical length suggests that when the SWCNT length is greater than the critical length, the charge transport behavior of the SWCNT thin film is dominated by intra-tube/bundle transport, and when SWCNT length is smaller than the critical length, it is dominated by inter- tube/bundle transport/tunneling.

Given the physical significance of T_0, one may use it as an indicator for the evaluation of the quality of transparent and conducting SWCNT thin films. Gruner et al.[25] have suggested using the quantity of σ_{ac}/σ_{dc} – the ratio of the optical conductivity to the DC conductivity as the quality indicator for evaluating SWCNT thin films. For a given SWCNT thin film, the smaller the σ_{ac}/σ_{dc}, the better its quality. By measuring the sheet resistance R and the optical transmission $T\%$ of SWCNT thin film, the quality σ_{ac}/σ_{dc} can be determined by

$$T\% = \frac{1}{\left(1 + \frac{2\pi}{cR}\frac{\sigma_{ac}}{\sigma_{dc}}\right)^2} \quad (5)$$

where c is the speed of light. With eq 5, the quality indicator σ_{ac}/σ_{dc} for all the SWCNT thin films prepared in this study was evaluated and compared with the 3D VRH parameter T_0. A power law relationship $T_0 = 968.4 \times (2\pi/c \times \sigma_{ac}/\sigma_{dc})^{0.65}$ is found existing between the Gruner's quality indicator σ_{ac}/σ_{dc} and the 3D VRH parameter T_0, as shown in Figure 6d.

After examining the effect of SWCNT structures on T_0, we now turn to the pre-exponential factor R_0 and σ_0. Equation 4b indicates that R_0 is inversely proportional to the optical absorbance A of SWCNT thin films. This relationship was confirmed experimentally, and the results are shown in Figure 7a, in which R_0 is plotted against the optical absorbance A at 550 nm for all the SWCNT thin films. Clearly, the experimentally determined data points of R_0 versus A can be nicely fitted by a theoretical relationship $R_0 = 1.7182/A$. The noticeable but slight data scattering around $R_0 = 1.7182/A$ as shown in Figure 7a suggest that the coefficient of $1/A - \varepsilon c/\sigma_0$ (eq 4b) has a relatively weak dependence on the processing conditions or the structures/morphologies of SWCNT thin films and can be approximated by a constant value of $\varepsilon(550\ \text{nm})c/\sigma_0 = 1.7182\ \Omega\ K^{-1/2}$. Here, $\varepsilon(550\ \text{nm})$ emphasizes that the optical absorption cross-section is evaluated at 550 nm wavelength. Otherwise, the numerical coefficient of the inverse relationship between R_0 and A should be accordingly changed. Unless the electronic structure of SWCNTs is severely modified, e.g., by chemical functionalization, the optical absorption cross-section ε of the SWCNT thin film should be independent of the changes of SWCNT structures induced by sonication and centrifugation process. Therefore, one may expect that the pre-exponential factor σ_0 is inversely proportional to the packing density c of SWCNTs in the thin film. This is a reasonable result, if one considers that $\sigma_0 \propto \sqrt{N(E_F)}$ (eq 3a), and the density of states of SWCNT thin film increases

dx.doi.org/10.1021/la401264r | Langmuir 2013, 29, 8694–8702

with increasing the SWCNT packing density. With the relationship $\varepsilon c/\sigma_0 = 1.7182\ \Omega K^{-1/2}$, one may readily evaluate the pre-exponential factor σ_0 if the SWCNT packing density is known. By using the absorption cross-section of SWCNTs at 550 nm ($1.55 \pm 0.12 \times 10^{-18}$ cm^2/C-atom[35]) and assuming the density of SWCNT thin film as 0.75 g/cm^3, which corresponds to a ~ 50% void content if the SWCNT density is taken as 1.5 g/cm^3,[29] we can estimate the value of σ_0 as $3.4 \times 10^4\ \Omega^{-1}$ cm^{-1} K$^{1/2}$.

By inspecting eqs 3a and 3b and using the experimentally established relationship $\varepsilon(550\ \text{nm})c/\sigma_0 = 1.7182\ \Omega\ K^{-1/2}$, we have the formula

$$\xi = \frac{0.0648}{\varepsilon(550\ \text{nm})c\sqrt{T_0}} \tag{6}$$

which allows one to readily evaluate the electron localization length of SWCNT thin films from T_0, if the packing density c is known. The numerical coefficient in eq 6 was evaluated by taking the G-band vibration mode of SWCNT (1593 cm^{-1}) as the phonon frequency $\nu_{ph} = 4.78 \times 10^{13}$ s^{-1}. Without assuming the SWCNT packing density, we calculated the quantity ξc by using $\langle T_0 \rangle$. The results are plotted against the SWCNT length and shown in Figure 7b. Again, one can identify a critical SWCNT length of ~700 nm in Figure 7b. When the tube length is greater than 700 nm, the electron localization length of SWCNT thin film hardly depends on the tube length. However, for the SWCNT thin films formed by tubes with shorter length (<700 nm), a drastic decrease of the electron localization length is observed. At this stage, the physical significance of the critical length 700 nm is not clear. Future research will be pursued to resolve this issue.

CONCLUSIONS

Our previously developed PUM and DLS proves to be useful for quantitatively studying the processing−structure−electrical property relationship of SWCNT thin films. With assistance of PUM and DLS, SWCNT thin films fabricated by a scalable spray coating technique have been investigated for understanding the electronic transport mechanism of SWCNT thin films with tailored nanotube structure. A critical SWCNT length of ~700 nm has been identified, which divides the length-dependent electron localization of SWCNT thin films into two regimes. When SWCNT length is great than ~700 nm, the charge carrier localization hardly shows length dependence. However, when the SWCNT length is less than ~700 nm, the extent of charge carrier localization in SWCNT thin films decreases rapidly with decreasing the tube length. The results and methodology presented in our studies are highly valuable for further developing and optimizing SWCNT enabled multifunctional materials.

ASSOCIATED CONTENT

Supporting Information

Estimation of the SWCNT dispersion utilization efficiency in the SWCNT thin film fabrication process by spray coating technique. This material is available free of charge via the Internet at http://pubs.acs.org.

AUTHOR INFORMATION

Corresponding Author

*E-mail: liutao@eng.fsu.edu.

Author Contributions

The manuscript was written through contributions of all authors. All authors have given approval to the final version of the manuscript.

Notes

The authors declare no competing financial interest.

ACKNOWLEDGMENTS

T.L. and S.L. acknowledge the funding support provided by the Air Force Office of Scientific Research (AFOSR) and supervision by Dr. David S. Stargel. S.M.B. acknowledges support from NSF-DMR 1005293 and AGEP-GRS. The NHMFL where some of the work was carried out is supported by the NSF, the DOE, and the State of Florida.

REFERENCES

(1) Cao, Q.; Rogers, J. A. Ultrathin films of single-walled carbon nanotubes for electronics and sensors: A review of fundamental and applied aspects. *Adv. Mater.* **2009**, *21*, 29−53.
(2) Cao, Q.; Kim, H.; Pimparkar, N.; Kulkarni, J. P.; Wang, C.; Shim, M.; Roy, K.; Alam, M. A.; Rogers, J. A. Medium-scale carbon nanotube thin-film integrated circuits on flexible plastic substrates. *Nature* **2008**, *454*, 495−500.
(3) Gruner, G. Carbon nanotube films for transparent and plastic electronics. *J. Mater. Chem.* **2006**, *16*, 3533−3539.
(4) Kuttel, O. M.; Groening, O.; Emmenegger, C.; Schlapbach, L. Electron field emission from phase pure nanotube films grown in a methane/hydrogen plasma. *Appl. Phys. Lett.* **1998**, *73* (15), 2113−2115.
(5) Lee, S. W.; Kim, B. S.; Chen, S.; Yang, S. H.; Hammond, P. T. Layer-by-layer assembly of all carbon nanotube ultrathin films for electrochemical applications. *J. Am. Chem. Soc.* **2009**, *131*, 671−679.
(6) Dharap, P.; Li, Z. L.; Nagarajaiah, S.; Barrera, E. V. Nanotube film based on single-wall carbon nanotubes for strain sensing. *Nanotechnology* **2004**, *15*, 379−382.
(7) Sayago, I.; Terrado, E.; Lafuente, E.; Horrillo, M. C.; Maser, W. K.; Benito, A. M.; et al. Hydrogen sensors based on carbon nanotubes thin films. *Synth. Met.* **2005**, *148*, 15−19.
(8) Fuhrer, M. S.; Holmes, W.; Richards, P. L.; Delaney, P.; Louie, S. G.; Zettl, A. Nonlinear transport and localization in single-walled carbon nanotubes. *Synth. Met.* **1999**, *103*, 2529−2532.
(9) Liu, B.; Sundqvist, B.; Andersson, O.; Wagberg, T.; Nyeanchi, E. B.; Zhu, X.-M.; Zou, G. Electric resistance of single-walled-carbon nanotubes under hydrostatic pressure. *Solid State Commun.* **2001**, *118*, 31−36.
(10) Jaiswal, M.; Wang, W.; Fernando, K. A. S.; Sun, Y.-P.; Menon, R. Charge transport in transparent single-wall carbon nanotube networks. *J. Phys.: Condens. Matter* **2007**, *19*, 446006.
(11) Kymakis, E.; Amaratunga, G. A. J. Electrical properties of single-wall carbon nanotube-polymer composite films. *J. Appl. Phys.* **2006**, *99*, 084302.
(12) Yosida, Y.; Oguro, I. Variable range hopping conduction in bulk samples composed of single-walled carbon nanotubes. *J. Appl. Phys.* **1999**, *86*, 999−1003.
(13) Morgan, C.; Alemipour, Z.; Baxendale, M. Variable range hopping in oxygen-exposed single-wall carbon nanotube networks. *Phys. Status Solidi A* **2008**, *205*, 1394−1398.
(14) Kaiser, A. B. Electronic transport properties of conducting polymers and carbon nanotubes. *Rep. Prog. Phys.* **2001**, *64*, 1−49.
(15) Alan, B.; Kaiser, A. B.; Skakalova, V. Electronic conduction in polymers, carbon nanotubes and graphene. *Chem. Soc. Rev.* **2011**, *40*, 3786−3801.
(16) Skakalova, V.; Kaiser, A. B.; Woo, Y. S.; Roth, S. Electronic transport in carbon nanotubes: From individual nanotubes to thin and thick networks. *Phys. Rev. B* **2006**, *74*, 085403.

(17) Kaiser, A. B.; Skakalova, V.; Roth, S. Modeling conduction in carbon nanotube networks with different thickness, chemical treatment and irradiation. *Physica E* **2008**, *40*, 2311−2318.
(18) Skakalova, V.; Kaiser, A. B.; Osvath, Z.; Vertesy, G.; Biro, L. P.; Roth, S. Iron irradiation effects on conduction in single-wall carbon nanotube networks. *Appl. Phys. A: Mater. Sci. Process.* **2008**, *90*, 597−602.
(19) Yanagi, K.; Udoguchi, H.; Sagitani, S.; Oshima, Y.; Takenobu, T.; Kataura, H.; Ishida, T.; Matsuda, K.; Maniwa, Y. Transport mechanisms in metallic and semiconducting single-wall carbon nanotube networks. *ACS Nano* **2010**, *4*, 4027−4032.
(20) Shklovskii, B. I.; Efros, A. *Electronic Properties of Doped Semiconductors*; Springer-Verlag: Berlin, 1984.
(21) Mott, N. F.; Davis, E. A. *Electronic Processes in Non-crystalline Materials*, 2nd ed.; Clarendon: Oxford, U.K., 1979.
(22) Green, A. A.; Hersam, M. C. Colored semitransparent conductive coatings consisting of monodisperse metallic single-walled carbon nanotubes. *Nano Lett.* **2008**, *8* (5), 1417−1422.
(23) Meitl, M. A.; Zhou, Y. X.; Gaur, A.; Jeon, S.; Usrey, M. L.; Strano, M. S.; Rogers, J. A. Solution casting and transfer printing single-walled carbon nanotube films. *Nano Lett.* **2004**, *4* (9), 1643−1647.
(24) Spotnitz, M. E.; Ryan, D.; Stone, H. A. Dip coating for the alignment of carbon nanotubes on curved surfaces. *J. Mater. Chem.* **2004**, *14*, 1299−1302.
(25) Hu, L.; Hecht, D. S.; Gruner, G. Percolation in transparent and conducting carbon nanotube networks. *Nano Lett.* **2004**, *4* (12), 2513−2517.
(26) Hecht, D.; Hu, L. B.; Gruner, G. Conductivity scaling with bundle length and diameter in single walled carbon nanotube networks. *Appl. Phys. Lett.* **2006**, *89*, 133112.
(27) Shin, D. H.; Shim, H. C.; Song, J. W.; Kim, S.; Han, C. S. Conductivity of films made from single-walled carbon nanotubes in terms of bundle diameter. *Script. Mater.* **2009**, *60*, 607−610.
(28) Simien, D.; Fagan, J. A.; Luo, W.; Douglas, J. F.; Migler, K.; Obrzut, J. Influence of nanotube length on the optical and conductivity properties of thin single-wall carbon nanotube networks. *ACS Nano* **2008**, *2* (9), 1879−1884.
(29) Liu, T.; Luo, S. D.; Xiao, Z. W.; Zhang, C.; Wang, B. Preparative ultracentrifuge method for characterization of carbon nanotube dispersions. *J. Phys. Chem. C* **2008**, *112*, 19193−19202.
(30) Luo, S.; Liu, T.; Wang, B. Comparison of ultrasonication and microfluidization for high throughput and large-scale processing of SWCNT dispersions. *Carbon* **2010**, *48*, 2992−2994.
(31) Provencher, S. W. Inverse problems in polymer characterization-direct analysis of polydispersity with photon correlation spectroscopy. *Macromol. Chem. Phys.* **1979**, *180*, 201−209.
(32) Provencher, S. W. Contin - A general-purpose constrained regulation program for inverting noisy linear algebraic and integral-equations. *Comput. Phys. Commun.* **1982**, *27*, 229−242.
(33) Yamakawa, H. Viscoelastic properties of straight cylindrical macromolecules in dilute-solution. *Macromolecules* **1975**, *8*, 339−342.
(34) Luo, S.; Liu, T. Structure-property-processing relationships of single-wall carbon nanotube thin film piezoresistive sensors. *Carbon* **2013**, *59*, 315−324.
(35) Liu, T.; Xiao, Z.; Wang, B. The exfoliation of SWCNT bundles examined by simultaneous Raman scattering and photoluminescence spectroscopy. *Carbon* **2009**, *47*, 3529−3537.
(36) Heller, D. A.; Barone, P. W.; Swanson, J. P.; Mayrhofer, R. M.; Strano, M. S. Using Raman spectroscopy to elucidate the aggregation state of single-walled carbon annotates. *J. Phys. Chem. B* **2004**, *108*, 6905−6909.
(37) Mason, M.; Weaver, W. The settling of small particles in a fluid. *Phys. Rev.* **1924**, *23*, 412−426.
(38) Shiragami, N.; Kajiuchi, T. Precipitation of protein by ultracentrifuge with angle rotor 0.1. Model for sedimentation process. *Bioprocess Eng.* **1990**, *5*, 85−88.
(39) Thess, A.; Lee, R.; Nikolaev, P.; Dai, H.; Petit, P.; Robert, J.; Xu, C.; Lee, Y. H.; Kim, S. G.; Rinzler, A. G.; Colbert, D. T.; Scuseria, G. E.; Tomanek, D.; Fischer, J. E.; Smalley, R. E. Crystalline ropes of metallic carbon annotates. *Science* **1996**, *273*, 483−487.
(40) Philipse, A. P. The random contact equation and its implications for (colloidal) rods in packing, suspensions, and anisotropic powders. *Langmuir* **1996**, *12*, 1127−1133.
(41) Wouterse, A.; Luding, S.; Philipse, A. P. On contact numbers in random rod packings. *Granular Matter* **2009**, *11*, 169−177.
(42) Shiraishi, M.; Ata, M. Conduction mechanisms in single-walled carbon nanotubes. *Synth. Met.* **2002**, *128*, 235−239.
(43) Liu, B.; Sundqvist, B.; Li, D.; Zou, G. Resistivity and fractal structure in carbon nanotube networks. *J. Phys.: Condens. Matter* **2002**, *14*, 11125−11129.
(44) Li, Q.; Li, Y.; Zhang, X.; Chikkannanavar, S. B.; Zhao, Y.; Dangelewicz, A. M.; Zheng, L.; Doorn, S. K.; Jia, Q.; Peterson, D. E.; Arendt, P. N.; Zhu, Y. Structure-dependent electrical properties of carbon nanotube fibers. *Adv. Mater.* **2007**, *19*, 3358−3363.
(45) Bae, D. J.; Kim, K. S.; Park, Y. S.; Suh, E. K.; An, K. H.; Moon, J.; Lim, S. C.; Park, S. H.; Jeong, Y. H.; Lee, Y. H. Transport phenomena in an anisotropically aligned single-wall carbon nanotube film. *Phys. Rev. B* **2001**, *64*, 233401.
(46) Tanaka, T.; Mori, K.; Sano, E.; Fugetsu, B.; Yu, H. The Luttinger-liquid behavior in single-walled carbon nanotube networks. *Physica E* **2012**, *44*, 997−1001.
(47) Li, Z.; Kandel, H. R.; Dervishi, E.; Saini, V.; Xu, Y.; Biris, A. R.; Lupu, D.; Salamo, G. J.; Biris, A. S. Comparative study on different carbon nanotube materials in terms of transparent conductive coatings. *Langmuir* **2008**, *24*, 2655−2662.
(48) Paasch, G.; Lindner, T.; Scheinert, S. Variable range hopping as possible origin of a universal relation between conductivity and mobility in disordered organic semiconductors. *Synth. Met.* **2002**, *132*, 97−104.
(49) Nagels, P. Electronic transport in amorphous semiconductors. *Top. Appl. Phys.* **1985**, *36*, 113−158.